CORA Cork Open Research Archive
Cartlann Taighde Oscailte Chorcaí

Title	On-chip self-injection-locked gain-switched combs for flexible RF signal generation via photon–photon resonance
Authors	Dominguez-Castillejo, Diego;Venkatasubramani, Lakshmi Narayanan;Rajeswari, Gayatri Vasudevan;Prasad, Deepa;Atar, Fatih Bilge;Moehrle, Martin;Barry, Liam;Corbett, Brian
Publication date	2026-07-27
Original Citation	Dominguez-Castillejo, D, Venkatasubramani, L N, Rajeswari, G V, Prasad, D, Atar, F B, Moehrle, M, Barry, L & Corbett, B 2026, 'On-chip self-injection-locked gain-switched combs for flexible RF signal generation via photon–photon resonance', Journal of Lightwave Technology, vol. 44 , no. 18, pp. 8036-8045. https://doi.org/10.1109/JLT.2026.3717253
Type of publication	Article (peer-reviewed)
Link to publisher's version	https://www.scopus.com/pages/publications/105046085749 - 10.1109/JLT.2026.3717253
Rights	© 2026, the Authors. This work is licensed under a Creative Commons Attribution 4.0 License. - https://creativecommons.org/licenses/by/4.0/
Download date	2026-11-17 04:49:22
Item downloaded from	https://hdl.handle.net/10468/19284

UCC
University College Cork, Ireland
Coláiste na hOllscoile Corcaigh

On-Chip Self-Injection-Locked Gain-Switched Combs for Flexible RF Signal Generation via Photon–Photon Resonance

Diego Dominguez-Castillejo, *Graduate Student Member, IEEE*, Lakshmi Narayanan Venkatasubramani, *Member, IEEE*, Gayatri Vasudevan Rajeswari, Deepa Prasad, Fatih Bilge Atar, Martin Moehrle, Liam Barry, *Senior Member, IEEE*, and Brian Corbett

***Abstract*—Gain switching enables directly modulated lasers to generate ultrashort pulses with flexible repetition frequencies. By preserving pulse to pulse coherence, optical frequency combs can be generated. At high frequency repetition rates, external optical injection has proven to be effective in enhancing the spectral purity of these combs. However, the integration of such architectures remains challenging, and the maximum operating rate that these devices can reach is still limited by the relaxation oscillation frequency. In this study, we present a three-section laser that exploits photon-photon resonance as a mechanism to overcome these limitations. The laser includes an integrated external cavity that provides optical feedback to the gain section. This allows frequency combs to be generated with a flexible line spacing up to 30 GHz, limited by the equipment. Optical feedback drives the laser to operate in a self-injection locking regime, removing any need for optical external injection. An additional phase expansion scheme demonstrates the generation of frequency combs with a maximum spectral width of 150 GHz for a flatness window of 10 dB and a repetition rate of 30 GHz. Finally, frequency upconversion of a 2 GHz intermediate frequency signal to 28 GHz using a 30 GHz spaced comb is shown, demonstrating the potential of the proposed device as a flexible radio-frequency generator.**

Received 20 May 2026; revised 15 July 2026; accepted 23 July 2026. Date of publication 27 July 2026; date of current version 16 September 2026. This work was supported in part by European Union Horizon Europe research and innovation Programme through Marie Skłodowska-Curie under Grant Agreement 101073138 HORIZON-MSCA-2021-DN-01-01, in part by Taighde Éireann Research Ireland under Contract 12/RC/2276_P2, Contract 13/RC/2077_P2, and Contract 23/IRDIFB/11955, in part by HORIZON EUROPE European Innovation Council under Grant 101136762 (UNICO) and Grant 101137000 (M-Engine), in part by KDT Joint Undertaking (JU) through European Union's Horizon EU research and innovation programs and Austria, Belgium, Denmark, Finland, France, Germany, Greece, Hungary, Israel, Italy, Netherlands, Romania, Sweden, Switzerland, and Turkey, under Grant Agreement 101097296. *(Corresponding author: Diego Dominguez-Castillejo.)*

Diego Dominguez-Castillejo, Fatih Bilge Atar, and Brian Corbett are with Tyndall National Institute, University College Cork, T12R5CP Cork, Ireland (e-mail: diego.castillejo@tyndall.ie; fatih.atar@tyndall.ie; brian.corbett@tyndall.ie).

Lakshmi Narayanan Venkatasubramani, Deepa Prasad, and Liam Barry are with the Radio and Optical Communication Laboratory, School of Electronic Engineering, Dublin City University, 9 Dublin, Ireland (e-mail: lakshminarayanan.venkatasubramani@dcu.ie; deepa.prasad2@mail.dcu.ie; liam.barry@dcu.ie).

Gayatri Vasudevan Rajeswari and Martin Moehrle are with the Fraunhofer Institute for Telecommunication, Heinrich-Hertz-Institute, 10587 Berlin, Germany (e-mail: gayatri.vasudevan.rajeswari@hhi.fraunhofer.de; martin.moehrle@hhi.fraunhofer.de).

Color versions of one or more figures in this article are available at https://doi.org/10.1109/JLT.2026.3717253.

Digital Object Identifier 10.1109/JLT.2026.3717253

***Index Terms*—Frequency combs, integrated photonics, photon-photon resonance, self-injection locking.**

I. Introduction

MICROWAVE photonics (MWP) promises to be a potential solution to the growing need of generating carrier signals at ever-higher frequencies [1]. Properties such as immunity to electromagnetic interference and low transmission losses offer a reliable alternative to the scaling problems exhibited by conventional electronic systems at high frequencies [2]. Furthermore, by operating in the optical spectrum, it is straightforward to generate low phase-noise mm-wave signals through opto-electronic downconversion schemes [2], [3], [4]. However, it is also essential that these solutions meet the current requirements for increasingly smaller, lighter and power-efficient (SWaP) devices. In this context, photonic integration is key. Thanks to recent advances in heterogeneous integration techniques, the first MWP on-chip systems have been demonstrated [5], [6], opening the door to the potential scaling of this technology and the development of more compact and robust solutions.

The generation of RF signals utilising optical frequency combs (OFCs) offers a highly scalable alternative to traditional methods such as optical heterodyning using two uncorrelated lasers. The latter one produces a downconverted signal by beating two lasers at different optical frequencies, causing both sources to contribute to the noise of the resulting RF signal. In contrast, OFCs are simply sets of equidistant frequencies in the optical domain produced by a common noise source, i.e. a single laser source, exhibiting a high degree of phase correlation. Such property makes OFCs suitable to replace a number of distributed feedback (DFB) lasers in certain MWP applications [7], [8].

Mode-locked combs [9] and Kerr combs [10] have demonstrated strong performance as generators of high spectral purity signals. These combs exhibit a broad spectral range, facilitating the generation of frequencies even in the THz band. However, they have a discontinuous operating frequency range, as they depend directly on the effective cavity length or the free spectral range (FSR) of the ring, respectively. Therefore, if the FSR of these combs needs to be reduced, their dimensions must be increased, making their integration into a compact system more challenging for currently available foundry processes [11].

© 2026 The Authors. This work is licensed under a Creative Commons Attribution 4.0 License. For more information, see https://creativecommons.org/licenses/by/4.0/

A highly flexible and simple alternative are gain-switched laser combs [12]. This technique is based on the direct modulation of a laser, usually single-mode, by means of a sinusoidal signal. As a result of this modulation, the laser switches between ON and OFF states at a frequency determined by the sine wave, generating ultrashort pulses of the order of picoseconds [13]. In recent decades, these combs have been extensively studied, exhibiting a flexible FSR ranging from MHz [14], [15] to tens of GHz [16], [17]. Their monolithic integration has also been studied, with results demonstrating their potential scalability [18], [19], [20], [21], [22]. However, these architectures still present certain limitations that prevent gain-switched combs from becoming competitive integrated RF generators.

In [18], [20], architectures based on master-slave configuration are presented where a narrow-linewidth laser (master) injects photons into the directly modulated laser (slave). At low repetition rates, this architecture prevents optical pulses from being generated by spontaneous emission, as the master laser provides stimulated photons to build up coherent pulses, producing a phase-coherent comb [12], [13]. On the other hand, at high frequency rates, optical injection presents a different role. Instead of maintaining pulse coherence, it focuses on enhancing the spectral response of the combs, reducing their linewidth and phase noise [17]. However, these configurations are complex in an integrated system due to the lack of optical isolators. As a solution, the work presented in [21], [22] proposes a multi-section laser architecture that integrates both the master and slave lasers within the same cavity, reducing the system footprint. Although it is true that subsequent studies of these lasers show that a symmetric injection regime allows the comb to be spectrally broadened [23], they still present another limitation which is inherent to their own dynamics. In particular, gain-switched combs exhibit poor performance when modulated at repetition rates higher than the laser relaxation oscillation frequency [24]. In the case of [22], enhanced bandwidth operation of the comb is demonstrated at 3 GHz, showing a flexible operating range of only 1–10 GHz. Self-injection locking (SIL) has also been explored as an alternative to master-slave configurations. In [25], a DFB laser locked to a high-Q microresonator demonstrated a significant linewidth reduction in gain-switched comb lines, with linewidth narrowing being directly related to the Q-factor of the resonator. Nevertheless, no comb operation beyond 10 GHz was demonstrated and achieving fully monolithic integration of such resonator remains challenging. Therefore, these constraints highlight the need to design new integrated architectures capable of extending the frequency response of these lasers [26].

In the field of short-haul communications, several integrated laser architectures have been proposed for enhancing the resonant frequency under direct modulation [27], [28], [29], [30], [31], [32], [33]. In each of these architectures, an extended cavity is incorporated which provides feedback to the active section of the laser. As a result, resonance occurs due to strong modal interaction, which is capable of increasing the laser frequency response if properly engineered. This phenomenon is known as photon-photon resonance (PPR), through which an improvement in the laser small-signal response of up to 108 GHz has been achieved [34]. In [35] this phenomenon is exploited to generate frequency combs beyond the limit of the laser relaxation oscillation, achieving a 50 GHz comb. However, for such generation, assistance from an external master laser was required, and no detailed study was presented on the dependence of PPR and the spectral quality of the generated combs.

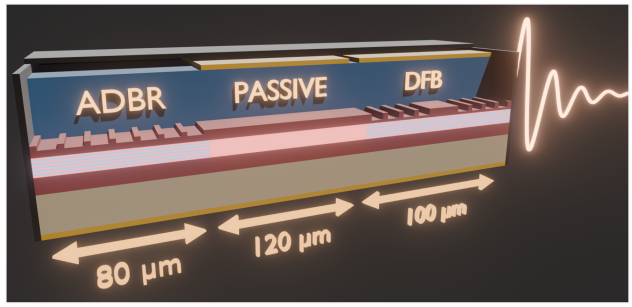

Fig. 1. Illustration of the 300 μm long multi-section laser. From left to right, laser is composed by an 80 μm active distributed Bragg reflector (ADBR), followed by a 120 μm passive waveguide and a 100 μm distributed feedback laser (DFB).

In this work, we demonstrate the flexible generation of RF signals using an integrated gain-switched comb source with enhanced modulation response via PPR. The multi-section laser employed in this paper has been previously investigated in the literature [31], [32], [33]. This device incorporates an extended cavity that provides integrated optical feedback, triggering an additional resonance in the laser. By exploiting this extra resonance, the laser frequency response is extended beyond 43.5 GHz when compared with conventional relaxation-oscillation limited semiconductor lasers. The spectral evolution of the device is analysed in detail, particularly the effect of PPR as a function of parameters such as current and temperature. At certain bias current points, the laser operates in a self-injection-locked regime, eliminating the need for an external laser and significantly reducing the complexity and footprint of the system. Furthermore, the generation of self-injection-locked flexible frequency combs via gain-switching up to 30 GHz is demonstrated, and the spectral quality of each of the electrical combs is analysed. The generated combs are then expanded through an electro-optic phase modulator, yielding a maximum comb width of 150 GHz within 10 dB flatness for a frequency spacing of 30 GHz. Finally, frequency upconversion is performed on an RF signal from a 2 GHz intermediate frequency to 28 GHz. To the best of our knowledge, this is the first demonstration of flexible RF signal generation through an on-chip self-injection-locked gain-switched laser.

II. Laser Characterisation

A. Laser Structure

The schematic of the laser is depicted in Fig. 1. The device follows a ridge-waveguide architecture comprising three monolithically integrated sections: a gain section, a passive waveguide, and an active distributed Bragg reflector (ADBR). The gain section consists of a quarter-wavelength-shifted DFB laser with a length of 100 μm, designed to operate in O-band.

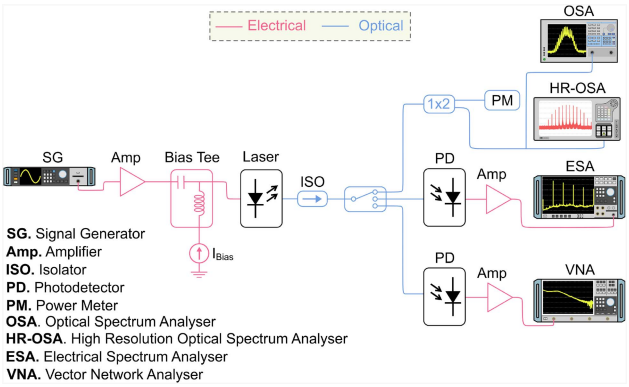

Fig. 2. Experimental setup for laser characterisation. **Upper.** LIV curves and spectral measurements. **Middle.** RF spectra and phase noise measurements. **Lower.** S21 measurements.

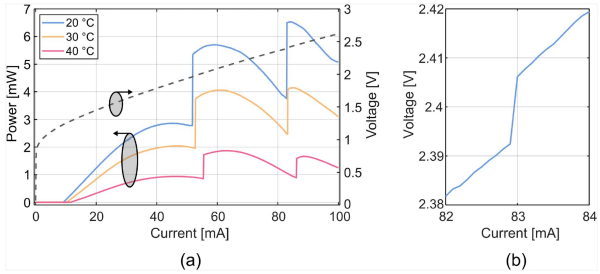

Fig. 3. LIV curves for different heat-sink temperatures (a). Detailed view of the voltage curve around second mode hop region for a heat-sink temperature of 20 °C (b).

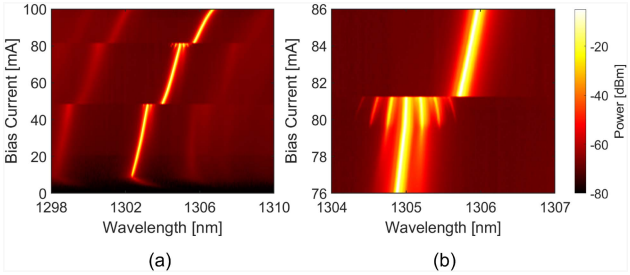

Fig. 4. Laser spectral map over the full operational region (a) and detailed view of the second mode hop region (b).

This is followed by a 120 μm passive waveguide that transmits the light to an 80 μm long ADBR. The latter acts as a partial mirror, reflecting a fraction of the optical power back to the DFB, thus forming an extended cavity. The resulting compound cavity introduces additional longitudinal modes that can interact with the main DFB lasing mode, giving rise to PPR at certain phase conditions. The waveguide includes a metal contact to adjust the phase of the feedback signal; nonetheless, its study is beyond the scope of this paper, and therefore it is not utilised. On the other hand, the ADBR structure consists of a uniformly spaced grating, sharing the same InGaAlAs multi-quantum-well (MQW) active layer as the DFB. Unlike the DFB section, the ADBR does not include a metal contact and remains unbiased, operating as a passive partial reflector rather than an active gain section. For an intended Bragg wavelength of 1305.5nm, the estimated coupling coefficients are $\kappa_{DFB} = 161$ cm^{-1} and $\kappa_{ADBR} = 40.25$ cm^{-1}, yielding reflectivities of 85.22 % and 9.69 %, respectively. Both laser facets are anti-reflection (AR) coated to suppress unwanted cavity feedback.

The device is packaged onto a diamond heat spreading submount. This assembly is attached to a copper heat sink, which is installed on a Peltier-controlled thermal regulator. Laser light is extracted by edge coupling, placing a lensed fibre at the facet of the DFB section. The laser is driven by a high-frequency signal ground (SG) probe (*Picoprobe Model 67 A*), with an operating bandwidth from DC to 67 GHz. However, it is important to note that the system suffers from impedance mismatch, since the probes have an impedance of 50 Ω, while the laser has a series resistance of 10 Ω. For this reason, approximately 67 % of the electrical signal is expected to be reflected, which significantly limits the maximum amplitude modulation than can be delivered to the system in order to guarantee secure operation of the instrumentation.

B. DC Characterisation

Fig. 2 illustrates the experimental setups employed to characterise the device. As an initial step, the fibre-coupled power was measured at different system temperatures. As shown in Fig. 3(a), the power curves were obtained as a function of the bias current of the DFB section. For simplicity, only one voltage-current curve is shown, corresponding to 20 °C. The laser threshold current is located around 9 mA, 10 mA, and 11.5 mA for temperatures of 20 °C, 30 °C, and 40 °C, respectively. The maximum power coupled to the lens ended single-mode fibre is 6.53 mW for a bias current of 84.2 mA and an operating temperature of 20 °C.

Two sharp kinks can be observed in all L-I curves, whose origin corresponds to laser longitudinal mode jumps [31], [32], [33]. This phenomenon occurs due to the optical feedback generated by the extended cavity. When working with a multisection laser, the modal distribution becomes complex, since both the modes corresponding to the DFB laser and the submodes generated by the delay of the extended cavity (passive waveguide + DBR) coexist inside the cavity. As the laser bias current increases, the phase of the feedback signal varies due to thermal effects, which, in certain occasions, leads to the coexistence of multiple longitudinal modes competing for the same gain, inducing the laser to operate in a non-linear regime, where different modes resonate between each other. When operating in this regime, both the phase and the injection feedback of the laser continue to vary, eventually causing a transition towards a more stable single-mode operation state, accompanied by a wavelength shift [36]. Every modal transition also causes a small increase in voltage (Fig. 3(b)), indicating a variation in the refractive index of the waveguide induced by a redistribution of the laser carriers [37].

Mode hops are shown in Fig. 4(a), which depicts the spectral evolution of the laser as a function of the injection current for a temperature of 20 °C. The spectra were obtained using an optical spectrum analyser (OSA, *Yokogawa AQ6370*) with a bandwidth

resolution of 0.02 nm. A typical red shift due to Joule heating in the device can be observed. As previously mentioned, the kinks in the L-I curves at 20 °C correspond to mode hops. These wavelength jumps occur at around 49 mA and 81 mA, with a spectral shift of approximately 0.8 nm. This value is proportional to a cavity length of ≈300 μm, which corresponds to the total device length.

Fig. 4(b) provides a detailed view of the second mode hop region. Initially, it can be observed that, in parallel with the main mode, a secondary mode emerges whose intensity increases as the current increases. This means that in this operating region, the system allows two modes to coexist. However, a greater increase in current causes the laser to transition to a period-one (P1) oscillation regime, a non-linear dynamic present in semiconductor lasers subject to external optical injection or optical feedback [36], [38], [39]. Additionally, it can be observed that the repetition frequency of this phenomenon decreases as the current increases, which is consistent with previous studies on PPR [29].

The relative intensity noise (RIN) of the laser was then characterised so as to observe the evolution of the PPR effect produced by the resonance of laser modes. For this experiment, a photodiode and a 50 GHz RF amplifier were used, as well as an electrical spectrum analyser (ESA, *Rohde & Schwarz FSW50*). External noise sources were subtracted from the system, isolating the intrinsic noise of the laser.

Fig. 5(a) shows the processed RIN measurements for bias currents close to the second mode hop region of the laser at a temperature of 20 °C. The laser powered at 78 mA shows a frequency *plateau* in the range of 30 GHz to 50 GHz. However, when the current is increased to 80 mA, the interaction between modes increases significantly, showing a pronounced peak around 40 GHz, which relates to the PPR frequency. This peak reaches its maximum value at 81 mA, where the sideband intensity is maximum, with a slight shift of the resonance frequency to lower values. An additional increase of 1 mA causes the resonance frequency to drop drastically to 15 GHz, indicating that the laser has mode hopped and therefore exhibits single-mode emission again. In this operating regime, the frequency no longer corresponds to the PPR, but is determined by the relaxation oscillations of the DFB section. Fig. 5(b) shows the high resolution optical spectra for each of the currents at which the RIN measurements were obtained. Each measurement was acquired by means of a high resolution OSA (HR-OSA, *APEX OSA-AP6*) with an optical resolution of 0.04 pm.

All RIN measurements show an additional periodic component centred at 90 MHz, whose origin is attributed to the measurement system. The source of this parasitic frequency is related to the fibre coupling system, which causes a small portion of the light to be reflected back to the laser. This frequency is proportional to a fibre length of approximately one metre, which corresponds to the length of the lensed fibre before it is connected to an optical isolator. The amplitude of this resonance depends on the bias current, given that the greater the number of spectral lines, the greater the optical beat product in the photodetector, magnifying the frequency response. This explains why the resonance is minimal at 82 mA, where the laser operates in single-mode mode emission; and reaches its maximum at 81 mA, where the number of generated sidebands is maximum.

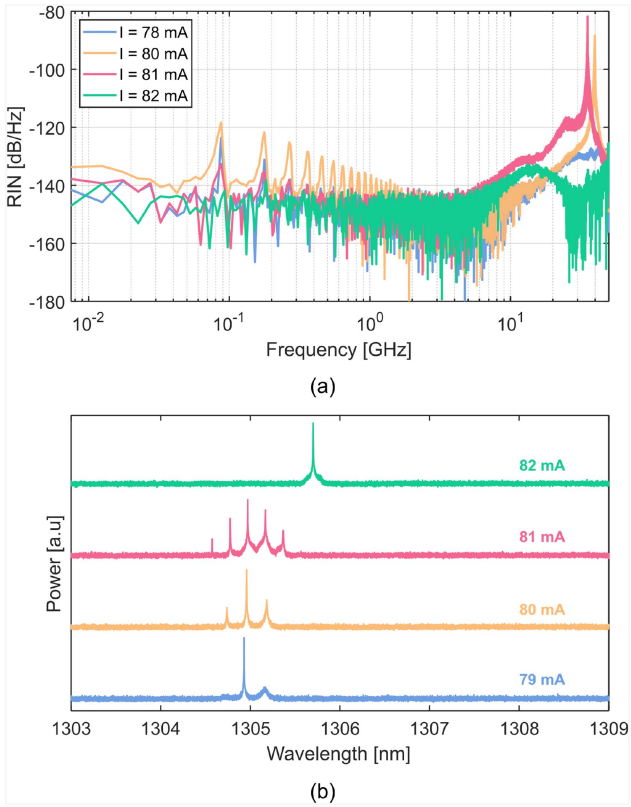

Fig. 5. RIN measurements at 20 °C for different bias currents (a) and their corresponding optical spectra (b).

C. RF Characterisation

The RF characterisation of the laser was then performed. As in the RIN measurement, the same photodetector and RF amplifier were used, replacing the ESA with a vector network analyser (VNA, *Rohde & Schwarz ZNB*). Port 1 was connected to the RF probes while Port 2 was connected to the electrical output of the RF amplifier, closing the circuit.

Figs. 6(a)–(c) show the frequency response maps of the laser as a function of bias current for temperatures of 20 °C, 30 °C, and 40 °C, respectively. The black dashed line delimits the 3 dB bandwidth of the laser, and its absence indicates that the laser response at that operating current exceeds the operating limit of the measurement system (i.e., 43.5 GHz).

As the operating temperature of the system increases, the frequency response of the device degrades. This is because at higher temperatures the differential gain of the device is reduced for the same bias current level, limiting the amplification of the cavity modes [28]. This means that in order to produce modal competition and thus magnify the frequency response of the laser, the mode separation must be reduced. Similarly, if the current is increased, the differential gain of the device increases

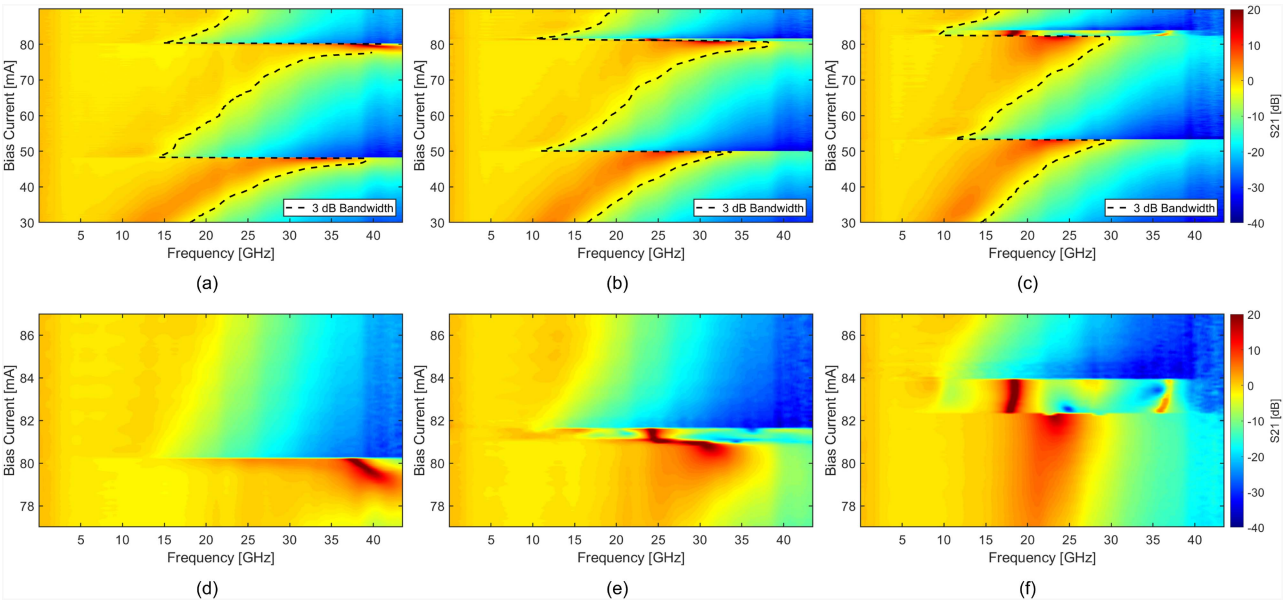

Fig. 6. Measured S21 maps at 20 °C (a), 30 °C (b) and 40 °C (c), and the corresponding detailed views of the second mode hopping point (d)-(f).

and the required distance between modes becomes greater again, increasing the frequency at which PPR occurs.

Figs. 6(d)–(f) detail the frequency dynamics of the device in the second mode hop region. At 20 °C, the PPR frequency presents a linear decreasing trend as a function of bias current. This indicates that, as the device current increases, the effective index increases, thus increasing the effective length of the extended cavity, ultimately causing the distance between modes to decrease progressively [28]. However, this trend varies significantly at 30 °C and 40 °C. At 30 °C an initial linearity is observed and is followed by an abrupt drop and subsequent locking of the frequency. At 40 °C this locking phenomenon occurs instantaneously. This behaviour suggests that at higher operating temperatures, the separation between modes is reduced, but not the optical injection rate that the laser receives due to the feedback from the extended cavity, which causes the laser to enter a new self-pulsating regime before performing another mode hop.

Fig. 7 shows the individual S21 plots of the laser at a temperature of 20 °C. Due to the deviations observed at low frequencies, which are attributed to the response of the electronic components of the setup, the plots have been normalised with respect to the *plateau* region that starts at 2 GHz. Similarly to the RIN measurements, the S21 curves corresponding to the second mode hopping region are reported. For bias currents of 65 mA, 72 mA, 79 mA, and 81 mA, 3 dB bandwidths of approximately 24 GHz, 27 GHz, >43.5 GHz (operating limit of the VNA), and 16 GHz were obtained, respectively. As previously described, the self-injection effect induced by the extended cavity generates a secondary resonance through the PPR mechanism. This phenomenon increases the modulation response as a function of the bias current due to the competition for a single gain that exists between two modes of the extended cavity. Once the mode hop has been triggered, the device transitions to a regime without

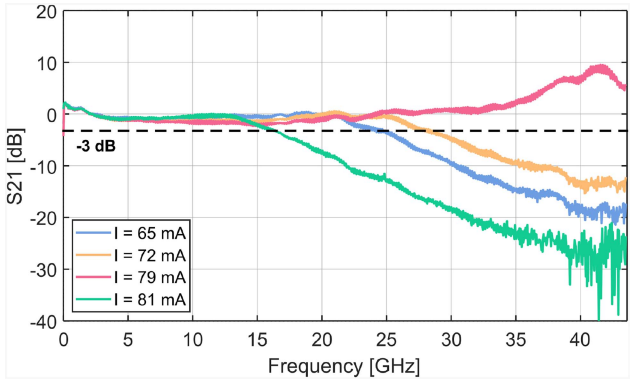

Fig. 7. Laser modulation responses at 20 °C for different bias currents around the second mode hop region. As current increases, the modulation response is enhanced due to a stronger PPR, until the laser mode hops (81 mA), showing a usual single-mode laser behaviour response.

modal competition, where the frequency response degrades until it is limited by the intrinsic relaxation oscillation frequency of the laser.

In view of these results, we conclude that the laser operates in two different regimes: a PPR-enhanced state, where optical feedback from the extended cavity enhances the frequency response of the laser; and a single DFB operation state, where the laser emission gets stabilised and it operates similarly to a single-section DFB laser. These two conditions are dictated by the feedback effect of the extended cavity, which causes the reinjected field to be in-phase or anti-phase with respect to the laser cavity mode under different bias points. It is the self-heating of the laser, and the resulting change in the effective cavity length what determines these phase-dependent operating conditions [40].

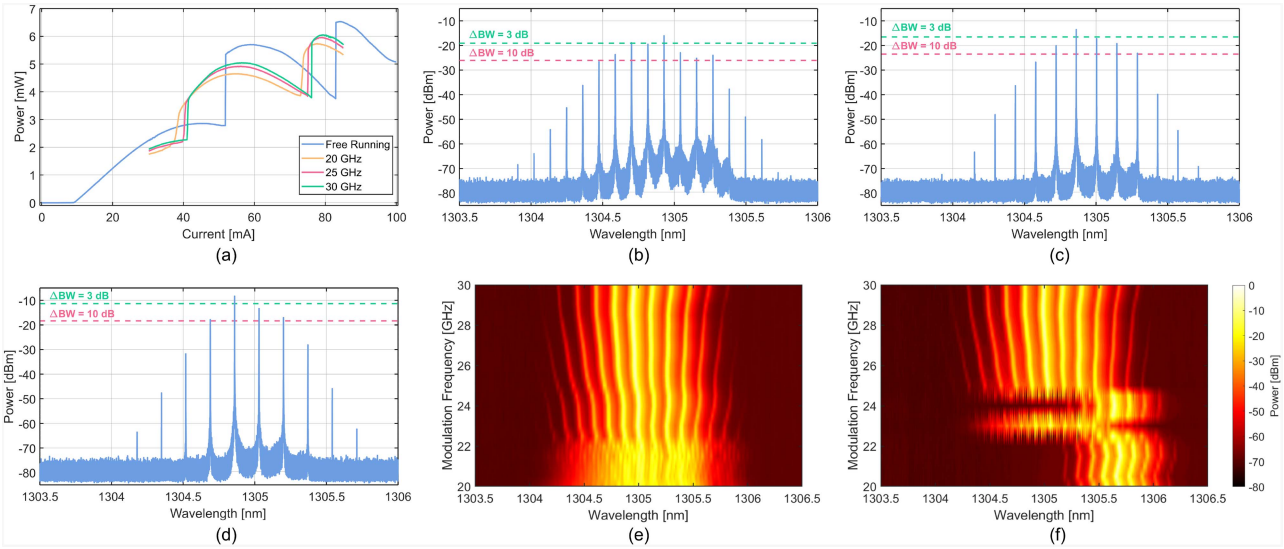

Fig. 8. L-I curves for different modulation amplitudes (a). Comb generation at 20 GHz for $I_{bias} = 69$ mA and $P_{mod} = 19$ dBm (b), 25 GHz for $I_{bias} = 73$ mA and $P_{mod} = 19$ dBm (c) and 30 GHz for $I_{bias} = 74$ mA and $P_{mod} = 18$ dBm (d). Evolution of the generated frequency combs as a function of the modulation frequency at 72 mA (e) and 74 mA (f).

III. Comb Generation

A. Gain-Switching

The results obtained from the device characterisation suggest that, thanks to the PPR, the laser is capable of extending its operating bandwidth beyond the physical limit imposed by relaxation oscillations of the sole DFB section. Consequently, it is possible to predict that, under gain-switched operation, the device will generate optical pulses and, therefore, OFCs with repetition rates higher than those achievable with a conventional laser. For this experiment, a signal generator (SG, *Rohde & Schwarz SMA100B*) with a maximum operating frequency of 40 GHz was used, whose amplified RF output was combined with the DC current using a bias-tee.

L-I measurements were performed under a sinusoidal modulation with an amplitude of 19 dBm at different repetition frequencies. As can be observed in Fig. 8(a), the kinks corresponding to the modulated L-I curves experience a significant shift towards lower bias. This phenomenon is more noticeable at lower frequencies, since the laser exhibits better performance at lower operating frequencies. This results in a less attenuated modulated signal at lower frequencies, which in turn produces a higher RMS value. It should be noted that although the 30 GHz curve and the free-running curve show an almost identical trend, the location of the kink is lower for the former, since the effective current received by the device under gain-switched operation is the sum of the DC component and the RMS value of the sinusoidal signal. As a result, mode-hops occur earlier at lower bias points.

After identifying the operating points where the PPR effect enhances the laser modulation response for different repetition frequencies, OFCs were obtained using a methodology similar to that reported in [12]. Sweeps of the modulation amplitude and DFB bias current were performed for different modulation frequencies, capturing the spectrum at each iteration. Finally, the results were post-processed to locate the frequency comb with the highest figure of merit, which was defined as the product of the 10 dB bandwidth of the comb, the SNR of the comb, and the number of lines in the comb. Fig. 8(b)–(d) shows the best combs for 20 GHz, 25 GHz, and 30 GHz, respectively. In each of the figures, the points at 3 dB (green dashed line) and 10 dB (red dashed line) are delimited with respect to the maximum point of the spectrum, obtaining 7, 5, and 4 comb lines within the margin delimited at 10 dB for the frequencies of 20 GHz, 25 GHz, and 30 GHz, respectively.

In light of these results, it is demonstrated that bias current control is critical when generating flexible frequency combs. As analysed above, each modulation frequency has a slightly different power contribution to the laser, which essentially shifts the mode hopping point. This shift causes comb generation to be selectively optimised, favouring certain modulation frequencies over others depending on the chosen bias point. This phenomenon is validated in Fig. 8(e)–(f), which shows the spectral evolution of the comb at different modulation frequencies for bias currents of 72 mA and 74 mA, respectively. In both cases, a shift towards blue is observed as the frequency increases, confirming that at higher modulation frequencies, the modulated signal suffers higher losses. This same reasoning explains why at 74 mA a frequency region is observed where the laser has already mode hopped. Controlling the phase of the feedback signal could suppress this bias current dependence, allowing to tune the mode hop region, and consequently accessing high frequency generation across a wider range of operating bias points. Future measurements employing a laser with 50 Ω termination could improve power delivery to the laser, enabling higher repetition rates and OFCs with a wider spectral response. Lastly, the oscillations observed in the emission wavelength of the comb are attributed to small changes in the forward resistance of the

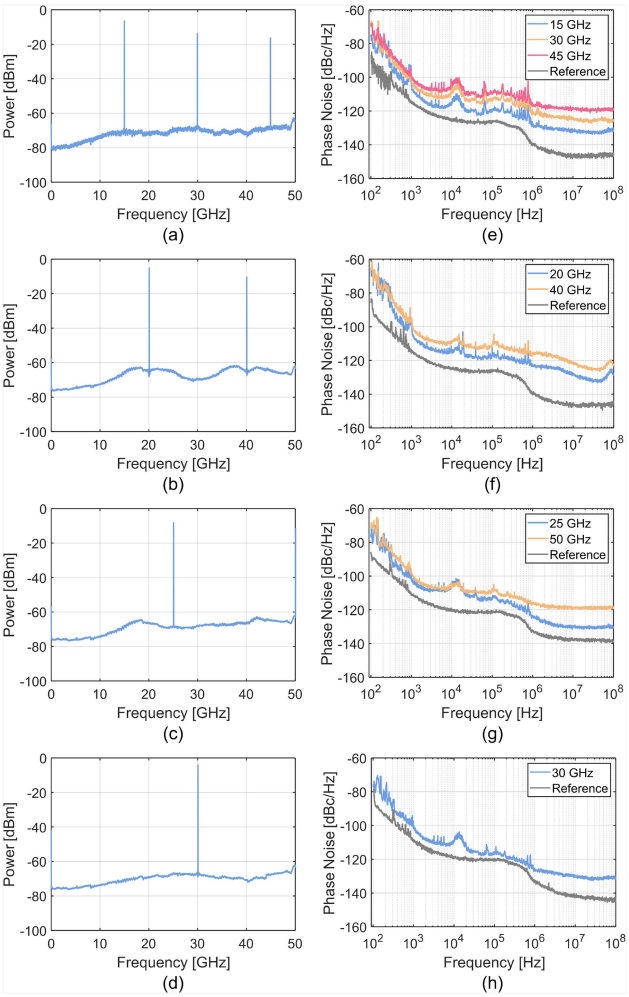

Fig. 9. RF spectrum measured at the photodiode output after feeding it with a gain-switched comb at repetition rates of 15 GHz (a), 20 GHz (b), 25 GHz (c) and 30 GHz (d), respectively. Phase noise measurements for each of the RF lines of the electrical combs (e-h). Grey curve represents the baseline performance of the RF signal source at each fundamental frequency.

laser, affecting the RF power delivery from the synthesiser to the laser.

B. Spectral Purity

Given the limited resolution of OSAs, an ESA was used to further analyse the characteristics of the different generated OFCs. To this end, laser output was connected to the same setup previously used for the RIN measurements (see Fig. 2). Various electrical combs with repetition frequencies of 15 GHz, 20 GHz, 25 GHz and 30 GHz were obtained, which are shown in Fig. 9 (a–d), respectively. The measurements were performed with a resolution bandwidth (RBW) of 1 MHz and a video bandwidth (VBW) of 1 kHz for a measurement span of 50 GHz.

The spectral purity of the generated tones was analysed by measuring the phase noise. The ESA built-in phase noise function was used, with 100 acquisitions per measurement taken over the frequency range of 100 Hz to 100 MHz. For each of the generated electrical combs, the phase noise of each spectral line

TABLE I
FREQUENCY NOISE OF FUNDAMENTAL FREQUENCIES (DBC/HZ)

		Frequency offset		
		1 kHz	100 kHz	10 MHz
Frequencies	15 GHz	-103.417	-120.480	-131.779
	20 GHz	-96.761	-116.784	-128.130
	25 GHz	-102.073	-113.746	-130.661
	30 GHz	-99.915	-115.949	-129.719

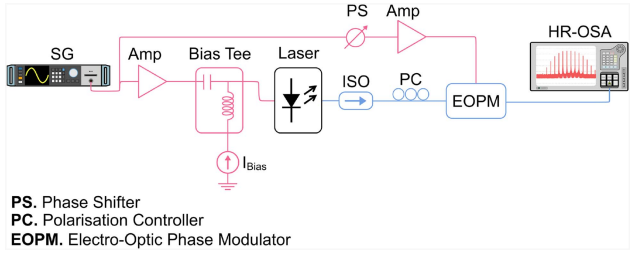

Fig. 10. Comb expansion setup through electro-optic phase modulation.

was obtained, i.e. the fundamental frequency and its respective harmonics. The results for the 15 GHz, 20 GHz, 25 GHz and 30 GHz combs are shown in Fig. 9(e)–(h). As can be observed, the results for the harmonics show an expected degradation in the phase noise response relative to the fundamental signal of the order of $20\log(\frac{f_2}{f_1})$, where f_1 is the fundamental frequency and f_2 its corresponding harmonic. However, the measurement for the 25 GHz comb does not exhibit this trend. It is believed that the reason for this discrepancy is due to a limitation in the ESA measurement, as its maximum operating range is 50 GHz and it is therefore operating at its operational limit. The spurious peaks appearing throughout the measurement are attributed to contributions from the various electronic components used in the measurement.

The first harmonic of the 15 GHz comb (i.e. 30 GHz) exhibits a phase noise of -113.426 dBc/Hz for 100 kHz and -123.835 dBc/Hz for 10 MHz. Meanwhile, the fundamental frequency of the 30 GHz comb shows an improvement in phase noise, with a phase noise of -115.949 dBc/Hz for 100 kHz and -129.719 dBc/Hz for 10 MHz. In view of these results, it can be confirmed that the higher the repetition rate of a comb, the better the phase noise performance obtained compared to combs generated at lower frequencies where their harmonics are to be used to generate signals of the same frequency.

As a reference for the reader, Table I shows the individual frequency noise values for the fundamental frequencies of the generated combs.

C. Comb Expansion

Employing an external phase modulator at the optical output of the laser is a frequently used technique for expanding the response of the generated combs [41]. Fig. 10 shows the setup used for frequency comb expansion. Firstly, the RF output is split

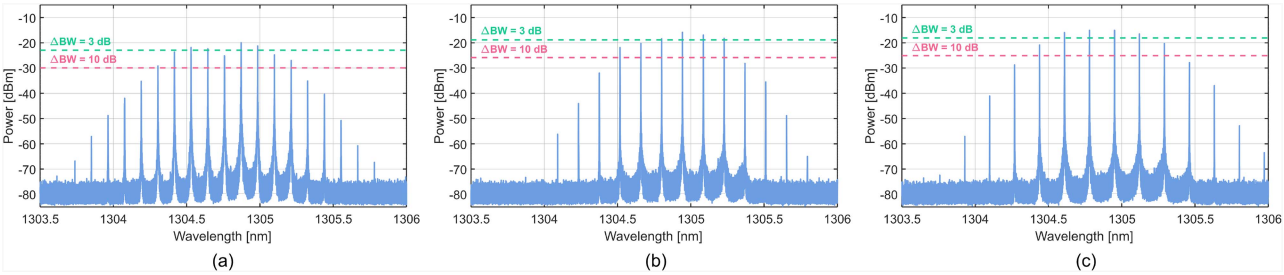

Fig. 11. Expanded comb generation at 20 GHz for $I_{bias} = 71$ mA and $P_{mod} = 21$ dBm (a), 25 GHz for $I_{bias} = 74$ mA and $P_{mod} = 21$ dBm (b) and 30GHz for $I_{bias} = 74$ mA and $P_{mod} = 21$ dBm (c).

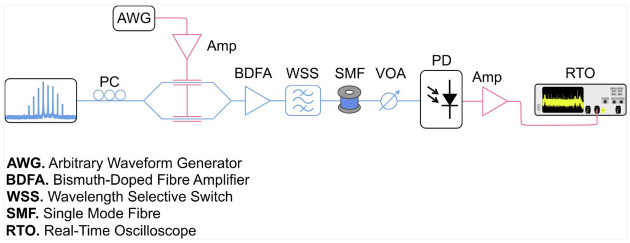

Fig. 12. Frequency upconversion system.

between both the laser and the electro-optic phase modulator (EOPM). An electrical phase shifter and an amplifier prior to the modulator are responsible for controlling the input phase and the modulation amplitude, respectively. When modulating a carrier with a sinusoidal signal, its spectrum exhibits the same behaviour as Bessel functions of the first kind [42]. Thus, if the line spacing of the comb is the same as the modulator frequency, sidebands are generated at the same spacing as the FSR of the comb. As a result, if the comb polarisation and phase shift are correctly adjusted, the sidebands interfere constructively, expanding its operating bandwidth. In this work, this technique achieves a 10 dB comb bandwidth beyond 150 GHz.

Fig. 11 shows the expanded combs for frequencies of 20 GHz, 25 GHz and 30 GHz, respectively. By manually adjusting the polarisation and the electrical phase, combs with a flat response and a greater number of operative comb lines were obtained. Therefore, if the device is packaged, higher modulation frequencies could be unlocked and subsequently expanded, making this device a flexible RF generator potentially capable of operating in the D-band.

IV. Upconversion Proof of Concept

To present the use of the comb source in systems applications, a system-level frequency upconversion of data translated from a 2 GHz intermediate frequency (IF) to a 28 GHz radio frequency is demonstrated. The schematic of the experimental setup is shown in Fig. 12. A 1 GBd 64-QAM signal from a PRBS15 bit sequence is generated offline as a part of transmitter-side digital signal processing (DSP). A raised cosine (RC) prototype filter is used to pulse-shape the signal with a 0.01 roll-off factor, reducing the electrical bandwidth to less than 1.5 GHz. The generated baseband signal is then digitally translated to a 2 GHz IF and loaded into an arbitrary waveform generator (AWG) operating at 30 GSa/s. The electrical signal is then amplified (using RF Amp 1) and set to drive the 30 GHz external Mach-Zehnder modulator (MZM), which modulates the lines of the optical comb with the amplified 1 GBd 64-QAM electrical signal centred at 2 GHz IF. The modulated signal was amplified using a bismuth-doped fibre amplifier (BDFA) with a gain of 17 dB to compensate for the modulation losses. Two of the modulated lines, separated by a 30 GHz comb spacing, were filtered using a programmable optical filter (Waveshaper 400B) before transmission over a single-mode fibre.

Figs. 13(a)–(b) show the optical spectrum of the free-running 30 GHz gain-switched comb and the filtered modulated carriers, respectively. The high resolution of the OSA (100 MHz RBW) enables the observation of the modulated signal at 2 GHz IF, with the modulated sidebands positioned exactly 28 GHz (and 32 GHz) from the neighbouring optical carrier. This confirms the target frequency translation to 28 GHz prior to detection. To estimate the receiver sensitivity, the signal power at the receiver (received optical power, ROP) was varied using a variable optical attenuator (VOA). The attenuated signal is then detected using a 70 GHz photodetector, amplified using a 16 dB gain RF amplifier and digitised using a 33 GHz real-time oscilloscope (RTO, 100 GSa/s).

On the receiver side, offline DSP first resamples the signal, and the 28 GHz-centred signal is digitally translated to baseband. A T/2-spaced 21 tap linear transversal feed-forward equaliser (FFE) is then applied to improve the performance. Fig. 13(c) shows the frequency domain spectrum of the captured signal as a function of the Fourier frequency. The plot shows the original signal centred at 2 GHz alongside the upconverted signal at 28 GHz and 32 GHz. The additional 32 GHz-centred signal and other spurious tones are observed due to the double-sideband nature of modulation and RTO clock and its harmonics, respectively. The performance of the upconverted signal is evaluated by measuring bit error ratio (BER) and error vector magnitude (EVM). The BER and EVM performance of the 1 GBd 64-QAM signal as a function of ROP is shown in Fig. 13(d). The performance across the ROP is observed to be within the standard hard-decision forward error correction (HD-FEC) BER limit of 3.8×10^{-3}, corresponding to an EVM limit of 8%. A similar performance is observed for the signal centred at 32 GHz, indicating flexibility in selecting the upconversion frequency. Constellation of the processed 28 GHz centred 1 GBd 64-QAM

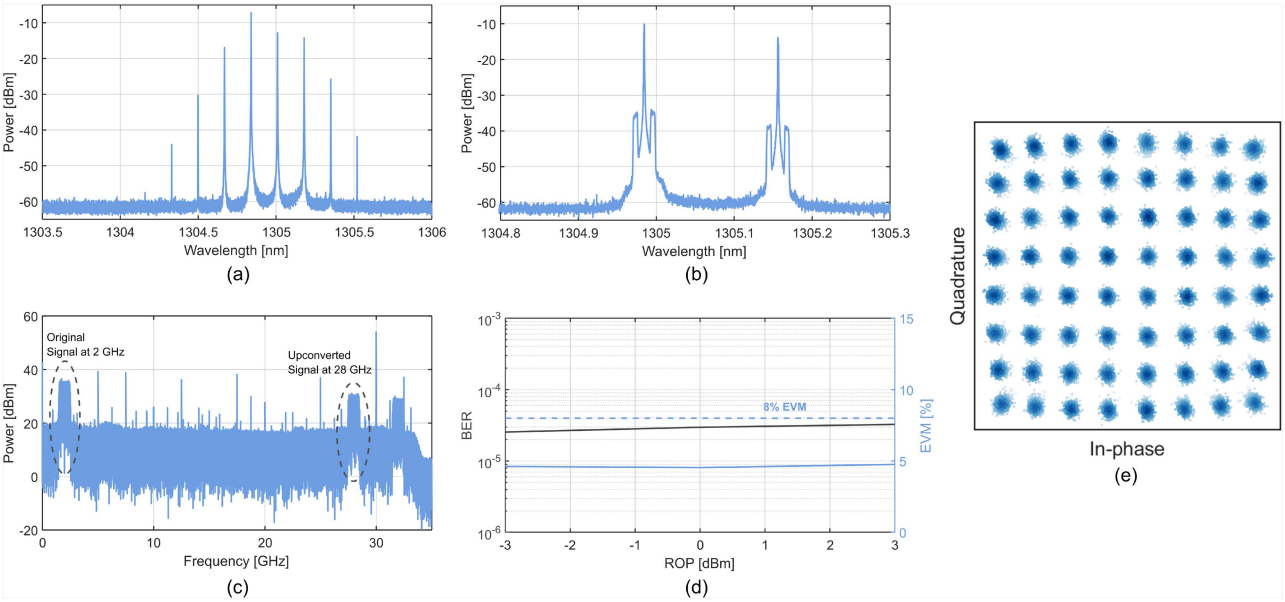

Fig. 13. Free-running gain-switched comb generated at 30 GHz with $I_{bias} = 74$ mA and $P_{mod} = 18$ dBm (a). Filtered optical carriers showing the 1 GBd 64-QAM modulation at an IF of 2 GHz (b). Electrical spectrum containing both the original and the upconverted RF signal (c). BER performance (black) and error vector magnitude (blue) of the 1 GBd 64-QAM signal upconverted to 28 GHz as a function of the received optical power (d). Constellation diagram of the upconverted 1 GBd 64-QAM signal at 28 GHz after demodulation (e).

signal at ROP of 0 dBm is shown in Fig. 13(e). The clear opening of the constellations is a visual measure of performance, indicating an arbitrarily low BER when FEC is employed.

V. Conclusion

In this work, the generation of flexible RF signals has been demonstrated using an integrated gain-switched comb source, which exploits PPR via an integrated extended cavity. Through this phenomenon, the frequency modulation response of the device is extended beyond 43.5 GHz, overcoming the intrinsic limitations imposed by laser dynamics. Consequently, the device generates highly-coherent frequency combs with a flexible repetition rate of up to 30 GHz. Further electro-optic phase expansion showcases a maximum comb width generation of 150 GHz for a repetition frequency of 30 GHz at a flatness of 10 dB. Additionally, the frequency upconversion of a 1 GBd 64-QAM signal from a 2 GHz IF to 28 GHz is performed as a proof of concept of the device potential for systems applications, yielding results below the HD-FEC limit.

It is therefore demonstrated that the implementation of the PPR is beneficial for the generation of gain-switched frequency combs and their potential applicability in the generation of RF signals. The use of the PPR not only causes the laser frequency response to extend to higher operating frequencies if properly engineered, but also, thanks to the laser architecture, ensures the laser to enter a self-injection locking state at certain bias points. Furthermore, its ability to generate flexible frequencies makes it a highly attractive option compared to other combs with fixed frequency spacing, such as mode-locked or Kerr combs.

Not having the device properly packaged results in the system modulation efficiency being limited due to the impedance mismatch between the laser and the RF tips. In order to prevent damage to the RF generation equipment caused by reflections, the modulation amplitude was limited, thereby affecting the final bandwidth of the generated comb. By encapsulating the device, it is possible to adapt the laser impedance, potentially enabling OFC generation with greater bandwidth and repetition rate. At the same time, the active control of the phase of the feedback signal would allow PPR to be exploited over a significantly wider bias current range. Together, these solutions could promote the use of this device as a practical microwave photonic RF generator capable of operating in the D-band.

References

[1] D. Marpaung, J. Yao, and J. Capmany, "Integrated microwave photonics," *Nature Photon.*, vol. 13, no. 2, pp. 80–90, 2019.
[2] Y. He et al., "Chip-scale high-performance photonic microwave oscillator," *Sci. Adv.*, vol. 10, no. 33, 2024, Art. no. eado9570.
[3] B. L. Krause, A. Lavrič, J. Tebart, A. Stöhr, and S. Preu, "Phase noise of an electro-optic terahertz comb," *Opt. Exp.*, vol. 32, no. 12, pp. 20948–20958, 2024.
[4] F. Van Dijk et al., "Integrated InP heterodyne millimeter wave transmitter," *IEEE Photon. Technol. Lett.*, vol. 26, no. 10, pp. 965–968, May 2014.
[5] F. B. Atar et al., "On-chip microwave photonic system through multi-component micro-transfer print integration," in *Proc. Int. Topical Meeting Microw. Photon.*, 2024, pp. 1–4.
[6] H. Deng et al., "Single-chip silicon photonic engine for analog optical and microwave signals processing," *Nature Commun.*, vol. 16, no. 1, 2025, Art. no. 5087.
[7] R. R. Kumar et al., "A 10-kHz intrinsic linewidth coupled extended-cavity DBR laser monolithically integrated on an InP platform," *Opt. Lett.*, vol. 47, no. 9, pp. 2346–2349, 2022.
[8] P. Primiani et al., "Silicon nitride bragg grating with joule thermal tuning for external cavity lasers," *IEEE Photon. Technol. Lett.*, vol. 31, no. 12, pp. 983–986, Jun. 2019.
[9] J. Gläsel et al., "Microwave photonics low phase noise RF comb generator for D-and J-band," *J. Lightw. Technol.*, vol. 44, no. 2, pp. 432–438, Jan. 2026.

[10] W. Liang et al., "High spectral purity kerr frequency comb radio frequency photonic oscillator," *Nature Commun.*, vol. 6, no. 1, 2015, Art. no. 7957.

[11] S. Cuyvers et al., "Low noise heterogeneous III-V-on-silicon-nitride mode-locked comb laser," *Laser Photon. Rev.*, vol. 15, no. 8, 2021, Art. no. 2000485.

[12] A. Rosado, A. Pérez-Serrano, J. M. G. Tijero, A. V. Gutierrez, L. Pesquera, and I. Esquivias, "Numerical and experimental analysis of optical frequency comb generation in gain-switched semiconductor lasers," *IEEE J. Quantum Electron.*, vol. 55, no. 6, pp. 1–12, Dec. 2019.

[13] P. Anandarajah et al., "Generation of coherent multicarrier signals by gain switching of discrete mode lasers," *IEEE Photon. J.*, vol. 3, no. 1, pp. 112–122, Feb. 2011.

[14] C. Quevedo-Galán, A. Rosado, A. Pérez-Serrano, J. M. G. Tijero, and I. Esquivias, "Dual-comb spectroscopy with enhanced resolution by pseudorandom phase modulation of gain-switched optical pulses," *J. Lightw. Technol.*, vol. 42, no. 10, pp. 3954–3962, May 2024.

[15] E. Russell, A. Ruth, B. Corbett, and F. Garcia Gunning, "Tunable dual optical frequency comb at 2 μm for CO_2 sensing," *Opt. Exp.*, vol. 31, no. 4, pp. 6304–6313, 2023.

[16] A. Delmade, L. P. Barry, D. Dass, and C. Browning, "Multi-frequency 5G NR millimeter-wave signal generation over analog RoF link using optical frequency combs," *Opt. Commun.*, vol. 545, 2023, Art. no. 129681.

[17] C. Browning et al., "Gain-switched optical frequency combs for future mobile radio-over-fiber millimeter-wave systems," *J. Lightw. Technol.*, vol. 36, no. 19, pp. 4602–4610, Oct. 2018.

[18] H. Othman et al., "Integrated comb laser with active de-multiplexer for spectrally sliced coherent receiver," *IEEE Photon. Technol. Lett.*, vol. 36, no. 12, pp. 787–790, Jun. 2024.

[19] P. Lopez-Querol, C. Quevedo-Galán, P. Castera, J. M. G. Tijero, I. Esquivias, and A. Perez-Serrano, "Monolithically integrated dual-comb generator based on gain switched semiconductor ring lasers," *Opt. Laser Technol.*, vol. 191, 2025, Art. no. 113317.

[20] A. Rosado, M. D. Gutierrez-Pascual, G. Jain, F. Smyth, and P. M. Anandarajah, "Dual optical frequency comb using a multi-functional PIC based on fully integrated injection locked gain-switched lasers," *Sci. Rep.*, vol. 16, 2025, Art. no. 3186.

[21] M. D. G. Pascual, V. Vujicic, J. Braddell, F. Smyth, P. Anandarajah, and L. Barry, "Photonic integrated gain switched optical frequency comb for spectrally efficient optical transmission systems," *IEEE Photon. J.*, vol. 9, no. 3, pp. 1–8, Jun. 2017.

[22] J. McCarthy and F. H. Peters, "On-chip gain switched frequency comb generation using a two sectioned single cavity laser without additional optical injection," *Opt. Exp.*, vol. 31, no. 18, pp. 29619–29626, 2023.

[23] D. O'Sullivan, J. McCarthy, E. Russell, Z. Jia, F. H. Peters, and B. Kelleher, "Optical frequency comb bandwidth enhancement of a monolithically integrated gain switched device," *Opt. Exp.*, vol. 33, no. 19, pp. 39991–39998, 2025.

[24] P. M. Anandarajah, S. P. Ó. Dúill, R. Zhou, and L. P. Barry, "Enhanced optical comb generation by gain-switching a single-mode semiconductor laser close to its relaxation oscillation frequency," *IEEE J. Sel. Topics Quantum Electron.*, vol. 21, no. 6, pp. 592–600, Nov./Dec. 2015.

[25] A. E. Shitikov, V. E. Lobanov, N. M. Kondratiev, A. S. Voloshin, E. A. Lonshakov, and I. A. Bilenko, "Self-injection locking of a gain-switched laser diode," *Phys. Rev. Appl.*, vol. 15, no. 6, 2021, Art. no. 064066.

[26] P. M. Anandarajah et al., "Flexible optical comb source for super channel systems," presented at the Opt. Fiber Commun. Conf., Anaheim, CA, USA, Mar. 17–21, 2013, Paper OTh3I–8.

[27] Y. Matsui, R. Schatz, D. Che, F. Khan, M. Kwakernaak, and T. Sudo, "Low-chirp isolator-free 65-GHz-bandwidth directly modulated lasers," *Nature Photon.*, vol. 15, no. 1, pp. 59–63, 2021.

[28] N. P. Diamantopoulos et al., "60GHz bandwidth directly modulated membrane III-V lasers on SiO_2/Si," *J. Lightw. Technol.*, vol. 40, no. 10, pp. 3299–3306, May 2022.

[29] N. P. Diamantopoulos et al., "16-channel directly modulated membrane III-V laser array on SiO_2/Si utilizing photon-photon resonance," *J. Lightw. Technol.*, vol. 42, no. 11, pp. 3997–4005, Jun. 2024.

[30] A. Zozulia, R. Schatz, S. Rihani, G. Berry, K. Williams, and Y. Jiao, "C-band directly modulated lasers with tunable photon–photon resonance in InP membrane," *IEEE J. Quantum Electron.*, vol. 60, no. 6, pp. 1–12, Dec. 2024.

[31] G. V. Rajeswari, M. Moehrle, F. Ehrensack, U. Troppenz, A. Sigmund, and M. Schell, "Novel $>$ 57GHz bandwidth O-band InGaAlAs MQW RW DFB," *Proc. SPIE*, vol. 12440, pp. 33–38, 2023.

[32] G. V. Rajeswari, M. Moehrle, A. Sigmund, and M. Schell, "Dual DFB for uncooled 40 Gbps and cooled 72 Gbps direct modulation," in *Proc. IEEE 29th Int. Semicond. Laser Conf.*, 2024, pp. 1–2.

[33] G. V. Rajeswari, M. Moehrle, A. Sigmund, and M. Schell, "Record 4 x 106 Gbps transmission from a directly modulated laser array using photon-photon resonance," presented at the Opt. Fiber Commun. Conf., San Francisco, CA, USA, Mar. 30–Apr. 3, 2025, Paper Tu3J–5.

[34] S. Yamaoka et al., "Directly modulated membrane lasers with 108 GHz bandwidth on a high-thermal-conductivity silicon carbide substrate," *Nature Photon.*, vol. 15, no. 1, pp. 28–35, 2021.

[35] Z. Liu, Y. Matsui, R. Schatz, F. Khan, M. Kwakernaak, and T. Sudo, "50-GHz repetition gain switching using a cavity-enhanced DFB laser assisted by optical injection locking," *J. Lightw. Technol.*, vol. 38, no. 7, pp. 1844–1850, Apr. 2020.

[36] S. Bauer et al., "Nonlinear dynamics of semiconductor lasers with active optical feedback," *Phys. Rev. E*, vol. 69, no. 1, 2004, Art. no. 016206.

[37] A. Daly et al., "Voltage spectroscopy and the operating state of an optically injected long wavelength VCSEL," *IEEE Photon. Technol. Lett.*, vol. 24, no. 14, pp. 1245–1247, Jul. 2012.

[38] S. Wieczorek, W. W. Chow, L. Chrostowski, and C. J. Chang-Hasnain, "Improved semiconductor-laser dynamics from induced population pulsation," *IEEE J. Quantum Electron.*, vol. 42, no. 6, pp. 552–562, Jun. 2006.

[39] A. Quirce, B. Kelleher, and A. Valle, "Optical injection locking of longitudinal modes in a discrete mode laser: Application in gain-switched optical frequency combs," *J. Lightw. Technol.*, vol. 42, no. 10, pp. 3799–3806, May 2024.

[40] Y. Liang, J. R. Coudevylle, H. Benisty, A. Ramdane, and A. Lupu, "Strong laser emission modulation by coherent perfect absorption inside complex-coupled distributed feedback laser diodes," *Small*, vol. 21, no. 1, 2025, Art. no. 2404388.

[41] R. Zhou, S. Latkowski, J. O'Carroll, R. Phelan, L. P. Barry, and P. Anandarajah, "40 nm wavelength tunable gain-switched optical comb source," *Opt. Exp.*, vol. 19, no. 26, pp. B415–B420, 2011.

[42] T. Kobayashi, H. Yao, K. Amano, Y. Fukushima, A. Morimoto, and T. Sueta, "Optical pulse compression using high-frequency electrooptic phase modulation," *IEEE J. Quantum Electron.*, vol. 24, no. 2, pp. 382–387, Feb. 1988.